Second harmonic generation in the near field and far field, a sensitive tool to probe crystalline homogeneity

L. Mahieu-Williame, Samuel Gresillon, Mireille Cuniot-Ponsard, Claude Boccara

Second harmonic generation in the near field and far field: A sensitive tool to probe crystalline homogeneity

Laurent Mahieu-Williame[a] and Samuel Grésillon
Laboratoire d'Optique Physique, University P. & M. Curie Paris 6, CNRS UPR A0005, ESPCI, 10 rue Vauquelin, 75231 Paris Cedex 5, France

Mireille Cuniot-Ponsard
Laboratoire Charles Fabry de l'Institut d'Optique, C.N.R.S. et Université Paris Sud, Campus Polytechnique, RD 128, 91127 Palaiseau Cedex, France

Claude Boccara
Laboratoire d'Optique Physique, University P. & M. Curie Paris 6, CNRS UPR A0005, ESPCI, 10 rue Vauquelin, 75231 Paris Cedex 5, France

(Received 29 November 2006; accepted 22 February 2007; published online 26 April 2007)

In order to probe crystalline orientation of $Sr_xBa_{1-x}Nb_2O_6$ (SBN:x) thin film, we have developed a detection scheme based on a scanning near-field optical microscope (SNOM). It is used to image simultaneously the fundamental and the second harmonic generation (SHG) of light by the sample under pulsed laser illumination. We demonstrate on SBN thin films that an apertureless SNOM can dramatically improve the resolution and the sensitivity of SNOM-SHG. Tip direction and focalization are the two crucial parameters in the SNOM-SHG experiments. Moreover, we show the ability of our setup to separate near field from far field contribution to the SHG. This is indeed very helpful in order to measure surface-SHG coefficients. © *2007 American Institute of Physics*.
[DOI: 10.1063/1.2719278]

I. INTRODUCTION

Despite its recent 20 year anniversary[1] nano-optics has been seldom combined with nonlinear optics.[2–5] In the framework of second harmonic generation (SHG) studies, neither signal nor resolution has been improved since the early articles[2,6] and they are still far from what could have been expected with respect to the recent progress of scanning near-field optical microscopy (SNOM).[7,8] SHG has been used recently in the near field using customized tips under specific illumination[9] to get a nanolight source and improve the resolution. But no progress has been made so far to improve SHG imaging in the near field despite the fact that SHG has applications ranging from solid state physics[10] to biomedical imaging.[11]

We propose in this paper a SNOM-SHG instrument with good resolution and high sensitivity, and show with the characterization of the crystalline orientation of nonlinear thin films the high potentiality of our setup. We prove that contrary to what has been presented and suggested recently,[9,12] our SNOM tip is not a SHG nanosource. It behaves like a scatterer of a given component of the electric field as we have shown recently.[13] This not only increases the sensitivity of structural SHG imaging but allows also to separate far-field SHG (generated in the bulk) from near-field SHG (generated close to the surface), which is a first step toward pure surface-SHG measurements.

First, we describe the $Sr_xBa_{1-x}Nb_2O_6$ (SBN) thin film and its second order nonlinearity. The paper continues with the originality of the experimental setup and the results obtained on the SBN sample are presented. In order to explain the images obtained a discussion on the origin of the near-field signal in our setup follows with results taken from tip approach curves.

II. THE EXPERIMENT: SBN CRYSTAL AND SECOND HARMONIC GENERATION

Crystalline $Sr_xBa_{1-x}Nb_2O_6$ (SBN:x) is an excellent ferroelectric material which has been widely studied for holographic recording and optical processing. The monocrystalline tungsten bronze (TB) SBN solid solution exhibits one of the largest known linear electro-optic coefficients ($r_{33} \simeq 1340$ pm V^{-1} for SBN:0.75),[14,15] nearly two orders of magnitude larger than that of the primary electro-optic material $LiNbO_3$. Thin films of SBN are particularly attractive for their potential use as low voltage electro-optic waveguides. This potential application in integrated optics requires the control of the (001) oriented SBN growth on the substrate.

Second order nonlinear effect is a very sensitive tool to probe the orientation of crystalline structures.[10,16–18] As all ferroelectric crystals, SBN is noncentrosymmetric and can generate SHG under illumination with laser pulses.[19] As the tensor χ^2 governs the SHG efficiency, the signal depends on the angle between the crystallite axis and the direction of propagation of the laser beam.

In nonlinear crystallized thin films, only the electro-optic coefficients are of importance and phase matching is not necessary because the propagation length is much smaller than the wavelength. Using thin films allows increasing the weight of two-dimensional effects with respect to bulk state.

[a]Electronic mail: lwilliame@yahoo.fr

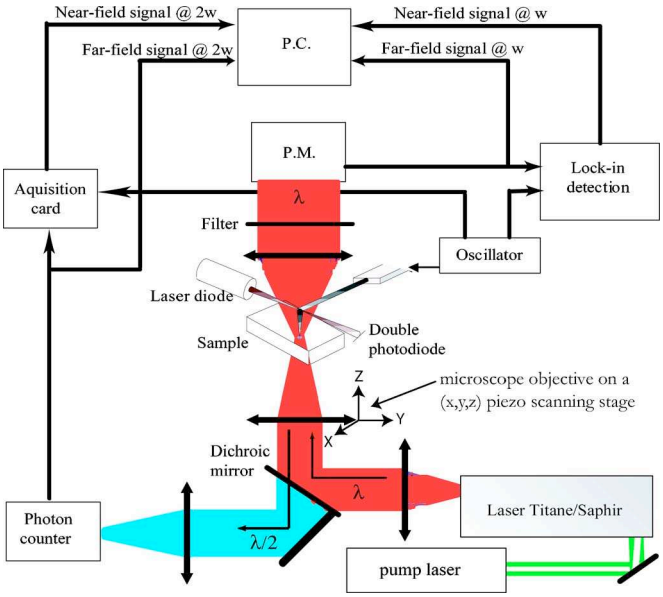

FIG. 1. (Color online) The experimental setup.

The SBN thin film (638 nm thick) investigated in this paper was prepared from a ceramic target $Sr_{0.5}Ba_{0.5}Nb_2O_6$ by using rf magnetron sputtering. It was deposited amorphous onto a (001) MgO substrate, then crystallized by annealing at 1050 K. X-ray analysis indicated that the film was highly (001) oriented, and formed of crystallites of about a 100 nm mean size, much smaller than the limit of resolution (R) of classical microscopy ($R \sim 250$ nm in the visible domain). To compare the orientation of the crystallites high resolution microscopes are needed and the resolution of SNOM is a perfect match.[20]

III. THE EXPERIMENTAL SETUP: NEAR-FIELD APERTURELESS MICROSCOPY

The microscope we used in the experiments described below scatters with the apex of a metallic tip the evanescent waves in the near field which contain subwavelength information.[21–23] The resolution of the microscope is directly related to the size of the metal tip end. Our metal tip is made by electrochemical erosion of a tungsten wire. The radius of the tip end is of the order of 10 nm.

In our experimental setup (Fig. 1) a pulsed Ti: sapphire laser centered at $\lambda_{ill} \simeq 800$ nm with a pulse width of 20 fs and a repetition rate of 80 MHz is focused onto the sample surface (the SBN film) by a microscope objective [Olympus 100× numerical aperture (NA)=0.8]. This microscope objective is on a three stage piezoelectric translator (x, y, and z). In transmission mode the x and y directions allow to center the illumination spot along the tip axis, and the z direction allows to optimize the SHG near-field signal. As we will show below, the optical SHG detector detects an interference product of the far field coming from the laser and the near field scattered by the tip. The SHG near-field signal is optimized when interferences of the collected far field and near field are constructive.

The tip oscillates vertically above the sample surface like in most tapping mode atomic force microscopes (AFMs). The scattered local field is modulated by the vertical oscillation of the tip. The sample and the tip are placed inside a microscope. Two detectors are used to collect the optical signal. The first one is a photomultiplier (PM) placed above the microscope and the sample. The upper light collection is made via a microscope objective (Olympus 50×, NA=0.5). With the help of one passband filter centered on $\lambda_{PM}=800$ nm, the PM collects the fundamental beam at $\lambda_{ill}=800$ nm. It is coupled with lock-in detection at the oscillating frequency of the tip. It allows us to recover the light scattered by the tip and to get rid of the far field coming from the illumination beam. The second detector placed below the sample is a photon counting detector (H7421). The collection is made via the 100× illumination objective and a $f=50$ mm lens. The photon counter (PC) stands after a dichroic beam splitter and several filters centered on $\lambda_{PC}=400$ nm (not shown). It allows us to collect the SHG at $\lambda_{SHG}=400$ nm. This collection mode is sometimes called inverse transmission detection. The photon counter is coupled to a data acquisition device, which plays the same role as the lock-in detection for the PM and allows separating the local scattered field (modulated by the tip) from the far field.[24,25]

Images are obtained by raster scanning horizontally the sample surface and simultaneously recording the SHG and fundamental near-field signals at each position of the sample. Furthermore, we make use of the tip vertical oscillation to record the sample topography. During the scan, the sample attached to the piezoelectric translator moves and the tip horizontal position stays constant with respect to the incident beam. This experimental configuration allows us to obtain simultaneously seven images of the same sample area: the topography (AFM), the far-field optical signal at the fundamental frequency, the far-field optical signal at the second harmonic frequency, the modulus and phase of the near-field optical signal (the signal scattered by the tip end) at the fundamental (angular frequency ω; wavelength λ_{ill}), and the modulus and phase of the near-field optical signal at the second harmonic frequency (angular frequency 2ω, wavelength $\lambda_{ill}/2$). Because the phase of the optical signal is mostly related to the error signal, we show also the optical phase of the near field to ensure that the modulus provides an accurate description of the optical near field and is not related to the topography of the sample surface.[26,27]

IV. IMAGES ON SBN THIN FILMS

Figures 2 and 3 show the seven different images obtained during a surface scan of a SBN thin film of about 600 nm in thickness resulting from seven or height crystallite layers. (The SBN crystallite mean size of the thin film studied here is of the order of 80 nm.) Images 2(b)–2(d) are the different optical images obtained by the PM at $\lambda_{ill}=800$ nm. Images 2(a) and 3(a) are identical and represent the film topography. Images 3(b)–3(d) represent the different optical images obtained by the photon counter at $\lambda_{SHG}=400$ nm. The optimum resolution is given by the displacement step of the translation stage, which is 60 nm here.

The applied laser energy density is 8×10^{-4} J cm^{-2} at the sample surface. The gain of the photomultiplier is set for a dc

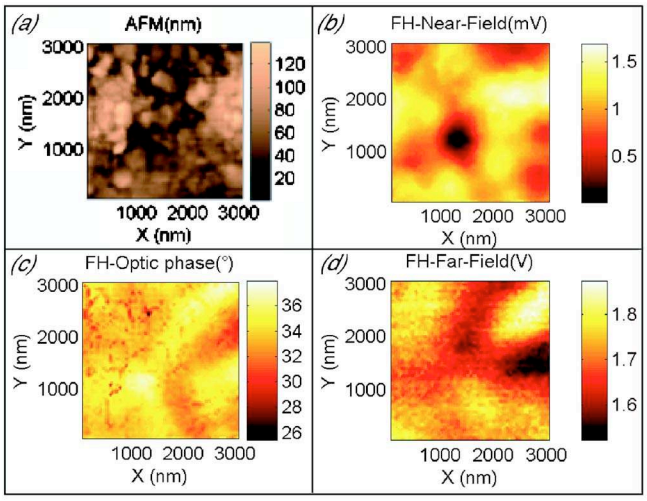

FIG. 2. (Color online) AFM image and fundamental harmonic optical images (3×3 μm^2) taken simultaneously on a SBN thin film. (a) Topographic image, (b) modulus of the near-field image, (c) optical phase of the near-field image, and (d) Far-field image.

output of around 1.7 V [Fig. 2(d)]. In our configuration the PM collects in the far zone the light transmitted by an ~1 μm^2 surface when the tip end scatters inside an ~10 nm^2 surface [for the tip end size, see the scanning electron microscopy (SEM) picture of a SNOM tip in Fig. 6(a)]. The near field scattered by the tip is then much smaller than the far-field output; this dc output is to a very good approximation the far-field signal. At the fundamental harmonic [Figs. 2(b) and 2(d)] the near field modulated and scattered by the tip is 10^{-3} smaller than the far field. This result is similar to the one already obtained with other apertureless SNOM setup and was the proof that an enhancement of the near-field signal arises, either by heterodyne detection inside the microscope or by enhancement of the electric field due to the tip geometry.[28–32]

Images obtained at ω (λ_{ill}=800 nm see Fig. 2) and 2ω (λ_{SHG}=400 nm, see Fig. 3) are different proving that the optical properties are different in the linear and nonlinear regimes. Whereas linear near-field image at ω [Fig. 2(b)] reveals diffraction-type structures linked to the sample topography as can be seen through the similarities between the phase of the optical signal [Fig. 2(c)] and the AFM image, the image at 2ω [Fig. 3(b)] provides another type of information. When the modulus of the near-field signal is strong, the phase [Fig. 3(c)] is locked. The recorded SHG near field is then purely from optical origin. On the contrary when the near-field signal is weak, the phase of the optical signal is random which proves that only noise is recorded in this area. The near-field image at 2ω [Fig. 3(b)] shows a bright spot three times more intense than the rest and is well correlated with a single crystallite group on the AFM image [Fig. 2(a) or 3(a)] and only with this one. This contrast reveals that this crystallite group is oriented differently than the other crystallites near the sample surface. The favorable orientation of this crystallite gives a higher weight at the high electro-optic coefficient of the SBN. Incidentally, the far field at 2ω [Fig. 2(d)] shows a bright spot four times more intense than the rest, which does not appear on the near-field image at 2ω. It suggests that a crystallite in the depth of the film has an orientation different than the surrounding crystallites. But this deep crystallite is too far away from the film surface to provide a near-field signature: it is in the far zone.

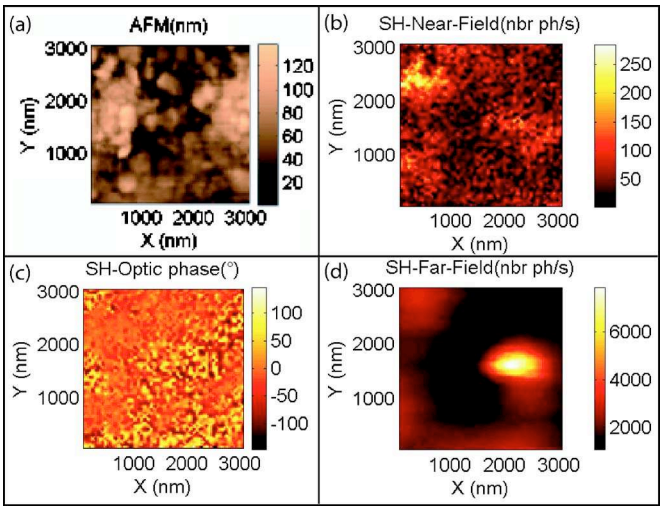

FIG. 3. (Color online) AFM image and second harmonic optic images (3×3 μm^2) taken simultaneously on a SBN thin film. (a) Topographic image [same image as Fig. 2(a)], (b) modulus of the near-field image, (c) optical phase of the near-field image, and (d) far-field image.

In order to better understand the difference between our far-field and our near-field measurements, a detailed description of the detection scheme and several tip approach curves are presented and commented below.

V. COMPARISON BETWEEN THE NEAR-FIELD AND THE FAR-FIELD IMAGES AT 2Ω

We have seen that the tip apex scatters the evanescent waves, which are confined on the sample surface. In the visible range, the near-field zone where the evanescent waves are preponderant over the propagating waves extends to ~70 nm above the sample surface.[7,33] For simplicity, we will call far zone the all volume that lies above this limit. In order to simulate the lock-in detection of the near field with the numerical signal of the photon counter at a fast repetition rate, we use an acquisition card (National Instrument, PCI-6602) which contains eight quartz clocks (at 80 MHz frequency or 12.5 ns pulse resolution). Four clocks open four temporal gates, each one recovering a successive quarter period of the oscillation of the tip. The four other clocks are counting photons arriving in each gate. For a typical oscillation period of 3 kHz, each gate is open during ~80 μs.

As the vertical oscillation amplitude of the tip is in the order of 150 nm, the tip stays typically half of the oscillation period in the near-field zone, and the other half in the far zone. The intensity of the propagating waves varies very slowly in the all volume occupied by the tip end during its movement. On the contrary, the intensity of the evanescent waves changes dramatically during the oscillation of the tip. The difference between the optical signals measured in each half period gives the fast varying process, a signal related to the scattered evanescent waves that is also called "near-field signal." The sum of the optical signal measured during both

half periods gives us the slow varying component of the electromagnetic (EM) field, which is here related to the far-field optical signal. Using four quarter periods instead of two half periods allows retrieving also the phase of the periodic scattered field with respect to the tip oscillation.

This behavior of the optical images explains why there is a strong difference between the near-field image of Fig. 3(b) and the far-field image of Fig. 3(d). The far-field images show only the slow varying components of the EM field along the propagation direction (Oz), most of which belong to propagating waves. On the other hand, near-field images are of fast varying EM field along Oz. These fast varying fields are mainly evanescent and belong to objects that are very close to the surface. The bright spot in image 3(b) (near field at 2ω) and the one in image 3(d) (far field at 2ω) are related to very different layers of the film. The first one originates from second harmonic generation by a single crystallite close to the surface. It is undoubtedly a single crystallite because its size matches the one of crystallites in the AFM image. The latter one belongs to deeply embedded single crystallite or group of crystallites inside the SBN film. Here the resolution of far-field microscopy does not allow a more precise determination of its size and position.

VI. TIP APPROACH AND ORIGIN OF THE NEAR-FIELD SIGNAL

To get a better insight into the near-field image at 2ω, a study of tip approaches is useful, because it allows understanding the physical origin of the signal scattered by the tip. A tip approach consists in decreasing the tip-sample distance (from few microns to the contact) while measuring the intensity of the near-field and far-field signals.

At first we realized tip approach at the fundamental frequency. Various authors have already shown[34,35] that this approach reveals an interference period $P=\lambda_{ill}/2$. Our studies, not shown here, revealed a similar result, $P=\lambda_{ill}/2=(400\pm10)$ nm and allow us to confirm that the vertical tip displacement (in the Oz direction) is well calibrated.

Simultaneously, we performed tip approach at the second harmonic. As we saw above, the numerical lock-in detection allows us to recover the fast varying component of the EM field along the propagation direction (Oz). But at any time during the oscillation period, far field and scattered EM field reach the detector and interference effects arise. Because of the long coherence length of laser light, in the order of 30 μm for the Ti: sapphire laser we used in the present experiment, interferences are possible even if the optical paths taken by the various light beams are more than several microns apart (typically the maximum distance between the tip and the sample surface). The four different waves that can reach the second harmonic detector (the photon counter) are the following, see Fig. 4: (A) a wave at 2ω coming directly from the SBN film, (B) a wave at 2ω directly generated by the tip, (C) a wave at 2ω generated by the SBN film and scattered by the tip towards the photon counter, and (D) a wave at ω scattered by the tip which generates a wave at 2ω in the SBN film.

Following previous papers that show that our near-field

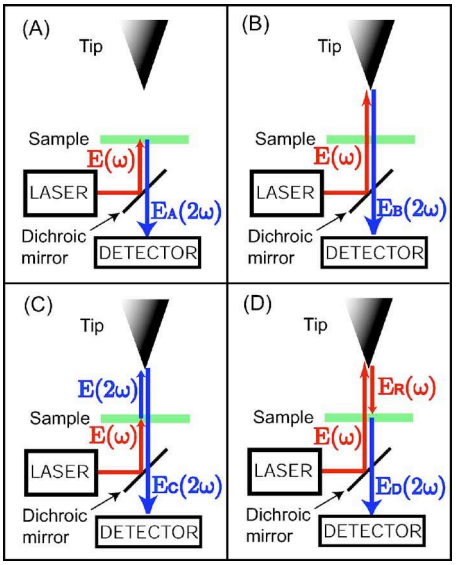

FIG. 4. (Color online) Four possible paths a wave at 2ω can reach the detector.

setup is only sensitive to the electric field,[13,36] the total intensity on the detector can be written in the following form where electric fields E_B, E_C, and E_D are modulated by the tip at the frequency $\omega_p\sim3$ kHz (the fast oscillation at the visible frequencies is omitted for simplicity) and c.c. stands for complex conjugate;

$$\begin{aligned} I_t &= |E_A + E_B\cos(\omega_p t) + E_C\cos(\omega_p t) + E_D\cos(\omega_p t)|^2 \\ &= |E_A|^2 + (|E_B|^2 + |E_C|^2 + |E_D|^2)\frac{\cos(2\omega_p t)+1}{2} \\ &\quad + (E_B E_C^* + E_B E_D^* + E_C E_D^* + \text{c.c.})\frac{\cos(2\omega_p t)+1}{2} \\ &\quad + (E_A E_B^* + E_A E_C^* + E_A E_D^* + \text{c.c.})\cos(\omega_p t). \end{aligned} \tag{1}$$

As the focalization length of the lens before the photon counter is large (50 nm), we approximate each wave arriving onto the detector by a plane wave. Because of the lock-in detection at the tip oscillation frequency ω_p, only the last term is extracted in the SHG near-field signal. Finally, the extracted SHG near-field signal is the last term of Eq. (1). Because of the phase and optical path difference between each field, three different interference periods exist depending on which couple of waves interfere, (A) with (B), (A) with (C), or (A) with (D). The periods are as follows: (A) with (B) gives $p_{AB}=\lambda/3\sim270$ nm, (A) with (C) gives $p_{AC}=\lambda/4\sim200$ nm, and (A) with (D) gives $p_{AD}=\lambda/2\sim400$ nm.

Figure 5 shows two tip approach curves on SBN sample obtained for different incident laser powers. Figure 5(a) was obtained for a laser energy density of 8×10^{-4} J cm^{-2} at the sample surface. This figure presents an interference period of $p\sim400$ nm$=p_{AD}$ which allows us to conclude that in the low power regime, our detection is mostly sensitive to the interference between far-field wave (A) and the wave (D) at ω scattered by the tip which generate a wave at 2ω at the sample surface. From the number of photons that reach the SHG detector, we can deduce the relative weight of process

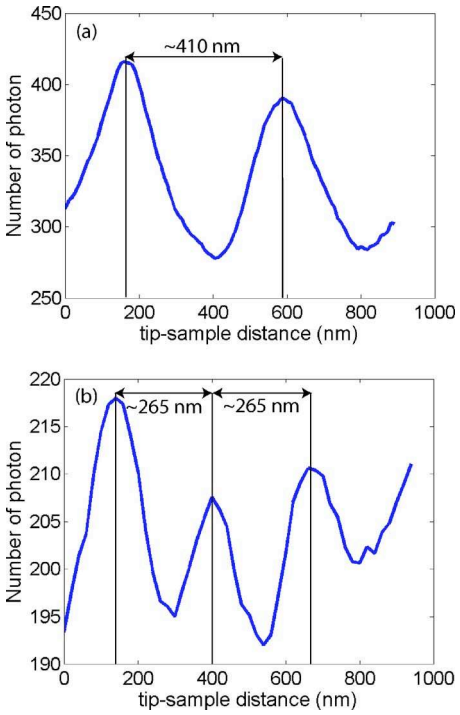

FIG. 5. (Color online) Intensities recorded at the photon counting detector as the tip approaches the surface sample. (a) For an incident laser energy density of 8×10^{-4} J cm^{-2} and (b) for an incident laser energy density of 10^{-3} J cm^{-2}.

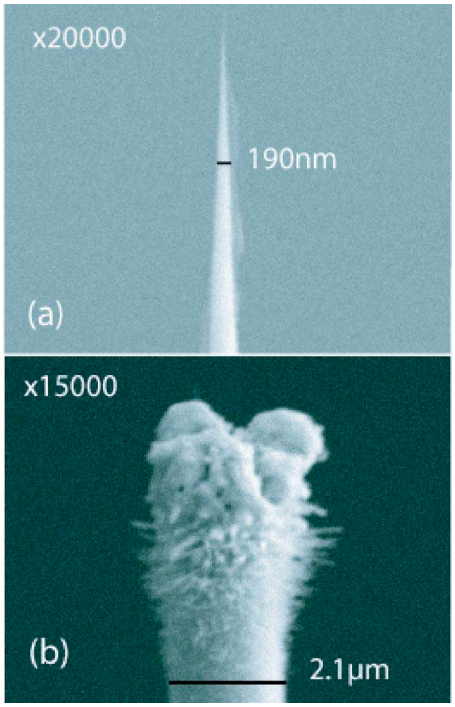

FIG. 6. (Color online) Scanning electron microscope images of tungsten tip. (a) A normal tip used in SHG-SNOM without high power laser illumination. (b) The tip after exposure to high illumination laser energy density ($>1.6\times10^{-3}$ J cm^{-2}).

(A) and (D). In our SHG detection, a rate of 3000 photons/s in far field is needed to get a near-field signal stronger than the noise of the detector (=40 photons/s).

Figure 5(a) is obtained for an average (far-field) signal of 4000 photons/s ($A\times A$) and the modulated part ($A\times D$) is 70 photons/s. It means that the process (D) sends only one useful photon per second to the detector. The near field scattered by the tip in the direction of the detector is between 10^{-4} and 10^{-3} times smaller than the far-field component. This ratio is fairly similar to the one obtained in the linear regime. It is a first hint that the tip does not act as a second harmonic source contrary to Refs. 9 and 12.

Figure 5(b) was obtained for an energy density of 10^{-3} J cm^{-2}. This figure presents an interference period of $p_{AB}=270$ nm and proves that the tip directly generates second harmonics. Despite the fact that tungsten is centrosymmetric, second harmonic is generated by the tip surface. This generation of second harmonic due to breaking of the symmetry at the interface is sometimes called surface-SHG (S-SHG).[37] This result was already demonstrated by several groups.[9,12] If one further increases the excitation energy density ($>1.6\times10^{-3}$ J cm^{-2}), the tip gets damaged as illustrated in Fig. 6(b).

VII. DISCUSSION

Due to the short propagation distance of the laser inside the SBN thin film, the detection of SHG and of near-field SHG is a big challenge. The high quality of the image is allowed, thanks to three important factors: (a) the presence of interference between far field and near field which plays the role of a heterodyne detection, (b) a very sensitive numerical lock-in detection to extract second harmonic generated in the near-field, and (c) the role of the tip that detects only one component of the EM field. More precisely indicated as follows.

- The illumination microscope objective which is below the sample (100×, see Fig. 1) is on piezoelectric translator which move it in x, y, and z directions. If the x and y directions are very important to center the illumination spot right on the tip, the z direction is even more important as it allow optimizing the SHG near-field signal by constructive interference with the far field on the detector. Moving vertically the microscope objective from a few hundred nanometers changes the near-field signal from zero for a destructive interference to the maximum for a constructive interference.
- Each point in the images is acquired in 1 s. As the oscillation frequency of the tip is around 3 kHz and the number of SHG photons is in the order of a few thousands, there is an average of one useful photon per period of oscillation of the tip. With the numerical lock-in we have developed, this is enough to realize a lock-in detection of the SHG.
- We have seen that the contrast in the SHG images depends on the angle between the optical axis of the crystallite and the direction of the electric field. The difficulty is that, due to the high numerical aperture of the microscope objective, the EM field at the focal point is scattered in many directions.[38–40] Fortunately the tip is more sensitive to the longitudinal component of the electric field. Many works on subwavelength holes[36,41] and on metal particles[13] have concluded that the tip scatters preferentially the longitudinal component of the electric field at the sample surface. The tip

plays the role of a *nanoantenna*[29,30,42] and amplifies the electric field component which has the direction of the tip axis (perpendicular to the sample surface). This explains why the contrast in the near-field image at 2ω [see Fig. 3(b)] depends so much on the direction of each crystallite.

VIII. CONCLUSION

Crystallite orientations of SBN thin film have been analyzed with a nanometric resolution using a developed optical instrument. This instrument consists in detecting the SHG optical response with a SNOM where the SHG efficiency depends of the angle between the optical axis of a crystallite and the laser beam propagation.

The fundamental and SHG optical responses are detected during the scan and compared with the optical phase. This ensures that the SHG optical response does not come from topographic artifact. The topographic image obtained by AFM correlates with the crystallite position in the optical image. This SNOM setup gives at least seven useful images of the same area during one scan. This is essential in order to better understand the near-field signal.

Tip approach is a good tool to get insight of the physical origin of SHG signal. A low laser power was used to get SHG signal coming from the SBN crystallites only. The optical contrast was obtained, thanks to the tip which amplifies the longitudinal component of the electric field and thanks to the interferences between far field and scattered near field, which give a very sensitive detection to retrieve one near-field photon per second. The tip can generate second harmonic for a higher laser power and could be used as a nanosource,[9,12] but warning should be made about the risk of destroying the tip.

This instrument with the SHG detection is well appropriated to reveal the crystallite orientation of noncentrosymmetric thin film. rf magnetron sputtering and annealing used to prepare the SBN thin films studied here reveal oneself as a very good technique because of the low presence of inhomogeneity in the crystallite orientation. Comparison between far-field SHG and near-field SHG allows differentiating between volume and surface effects. This could be a perfect tool to extract more information about the relative weight of surface and bulk χ^2 coefficients.

ACKNOWLEDGMENTS

The authors wish to thank Jean-Claude Rivoal for his everlasting support and confidence in this work. They also acknowledge Pr. Christian Ricolleau for the SEM images and very interesting discussions with Pr. Daniel van Labeke and Thierry Laroche on near-field SHG and Lionel Aigouy and Yannick De Wilde on near-field instrumentation. Financial support was provided by CNRS (crédits d'équipements 2004) and the Ministère Français de la Recherche (ACI photonique 2001).

[1] D. W. Pohl, W. Denk, and M. Lanz, Appl. Phys. Lett. **44**, 651 (1984).
[2] I. I. Smolyaninov, A. V. Zayats, and C. C. Davis, Phys. Rev. B **56**, 9290 (1997).
[3] D. Jakubczyk, Y. Shen, M. Lal, C. Friend, K. S. Kim, J. Swiatkiewicz, and P. N. Prasad, Opt. Lett. **24**, 151 (1999).
[4] A. V. Zayats and V. Sandoghdar, Opt. Commun. **178**, 245 (2000).
[5] S. I. Bozhevolnyi, J. Beermann, and V. Coello, Phys. Rev. Lett. **90**, 197403 (2003).
[6] S. I. Bozhevolnyi and T. Geisler, J. Opt. Soc. Am. A **15**, 2156 (1998).
[7] L. Novotny and B. Hecht, *Principles of Nano-Optics* (Cambridge University Press, Cambridge, 2006).
[8] Proceedings of the Ninth international Conference on Near Field Optics, Nanophotonics and Related Techniques, Lausanne, Switzerland, 10–15 September 2006 (unpublished).
[9] A. Bouhelier, M. Beversluis, A. Hartschuh, and L. Novotny, Phys. Rev. Lett. **90**, 013903 (2003).
[10] C. Ohlhoff, G. Lüpke, C. Meyer, and H. Kurz, Phys. Rev. B **55**, 4596 (1997).
[11] T. Pons, L. Moreaux, O. Mongin, M. Blanchard-Desce, and J. Mertz, J. Biomed. Opt. **8**, 428 (2003).
[12] M. Labardi, M. Zavelani-Rossi, D. Polli, G. Cerullo, M. Allegrini, S. De Silvestri, and O. Svelto, Appl. Phys. Lett. **86**, 031105 (2005).
[13] S. Grésillon, R. Lecaque, L. Williame, and J. C. Rivoal, Appl. Phys. B: Lasers Opt. **84**, 167 (2006).
[14] P. V. Lenzo, E. G. Spencer, and A. A. Ballman, Appl. Phys. Lett. **11**, 23 (1967).
[15] R. R. Neurgaonkar and W. K. Cory, J. Opt. Soc. Am. B **3**, 274 (1986).
[16] I. I. Smolyaninov, C. H. Lee, and C. C. Davis, Phys. Rev. Lett. **83**, 2429 (1999).
[17] V. Kirilyuk, A. Kirilyuk, and Th. Rasing, Appl. Phys. Lett. **70**, 2306 (1997).
[18] I. I. Smolyaninov, H. Y. Liang, C. H. Lee, C. C. Davis, S. Aggarwal, and R. Ramesh, Opt. Lett. **25**, 835 (2000).
[19] M. Horowitz, A. Bekker, and B. Fischer, Appl. Phys. Lett. **62**, 2619 (1993).
[20] D. W. Pohl, *Scanning Near-field Optical Microscopy* (Academic, New York, 1991).
[21] F. Zenhausern, M. P. O'Boyle, and H. K. Wickramasinghe, Appl. Phys. Lett. **65**, 1623 (1994).
[22] Y. Inouye and S. Kawata, Opt. Lett. **19**, 159 (1994).
[23] P. Gleyzes, A. C. Boccara, and R. Bachelot, Ultramicroscopy **57**, 318 (1995).
[24] T. J. Yang, G. A. Lessard, and S. R. Quake, Appl. Phys. Lett. **76**, 378 (2000).
[25] J. M. Gerton, L. A. Wade, G. A. Lessard, Z. Ma, and S. R. Quake, Phys. Rev. Lett. **93**, 180801 (2004).
[26] B. Hecht, H. Bielefeldt, Y. Inouye, D. W. Pohl, and L. Novotny, J. Appl. Phys. **81**, 2492 (1997).
[27] L. Billot *et al.*, Appl. Phys. Lett. **89**, 023105 (2006).
[28] L. Novotny, R. X. Bian, and X. Sunney Xie, Phys. Rev. Lett. **79**, 645 (1997).
[29] O. J. F. Martin and C. Girard, Appl. Phys. Lett. **70**, 705 (1997).
[30] H. Cory, A. C. Boccara, J. C. Rivoal, and A. Lahrech, Microwave Opt. Technol. Lett. **18**, 120 (1998).
[31] F. H'dhili, R. Bachelot, G. Lerondel, D. Barchiesi, and P. Royer, Appl. Phys. Lett. **79**, 4019 (2001).
[32] R. Hillenbrand, T. Taubner, and F. Keilmann, Nature (London) **418**, 159 (2002).
[33] *Le Champ Proche Optique*, edited by D. Courjon and C. Bainier (Springer, New York, 2001).
[34] A. Kramer, T. Hartmann, S. M. Stadler, and R. Guckenberger, Ultramicroscopy **61**, 191 (1995).
[35] R. Laddada, S. Benrezzak, P. M. Adam, G. Viardot, J. L. Bijeon, and P. Royer, Eur. Phys. J.: Appl. Phys. **6**, 171 (1999).
[36] S. Ducoutieux, S. Grésillon, J. C. Rivoal, C. Vanier, C. Bainier, D. Courjon, and H. Cory, Eur. Phys. J.: Appl. Phys. **26**, 35 (2004).
[37] T. Laroche, F. I. Baida, and D. Van Labeke, J. Opt. Soc. Am. B **22**, 1045 (2005).
[38] M. Lax, W. H. Louisell, and W. B. McKnight, Phys. Rev. A **11**, 1365 (1975).
[39] G. P. Agrawal and D. N. Pattanyak, J. Opt. Soc. Am. **69**, 575 (1979).
[40] L. W. Davis, Phys. Rev. A **19**, 177 (1979).
[41] F. Formanek, Y. De Wilde, and L. Aigouy, J. Appl. Phys. **93**, 9548 (2003).
[42] P. Muhlschlegel, H. J. Eisler, O. J. F. Martin, B. Hecht, and D. W. Pohl, Science **308**, 1607 (2005).